



Measurement of the $^{232}\text{Th}(n,f)$ cross section in the 1–200 MeV range at the CSNS Back-n

Zhi-Zhou Ren^{1,2} · Yi-Wei Yang² · Yong-Hao Chen^{3,4} · Rong Liu² · Bang-Jiao Ye¹ · Jie Wen² · Hai-Rui Guo⁵ · Zi-Jie Han² · Qi-Ping Chen² · Zhong-Wei Wen² · Wei-Li Sun⁵ · Han Yi^{3,4} · Xing-Yan Liu² · Tao Ye⁵ · Jiang-Bo Bai² · Qi An^{1,6} · Jie Bao⁷ · Yu Bao^{3,4} · Ping Cao^{6,8} · Hao-Lei Chen^{1,6} · Zhen Chen^{1,6} · Zeng-Qi Cui⁹ · Rui-Rui Fan^{3,4,10} · Chang-Qing Feng^{1,6} · Ke-Qing Gao^{3,4} · Xiao-Long Gao^{3,4} · Min-Hao Gu^{3,10} · Chang-Cai Han¹¹ · Guo-Zhu He⁷ · Yong-Cheng He^{3,4} · Yang Hong^{3,4,12} · Yi-Wei Hu⁹ · Han-Xiong Huang⁷ · Xi-Ru Huang^{1,6} · Hao-Yu Jiang⁹ · Wei Jiang^{3,4} · Zhi-Jie Jiang^{1,6} · Han-Tao Jing^{3,4} · Ling Kang^{3,4} · Bo Li^{3,4} · Chao Li^{1,6} · Jia-Wen Li^{6,13} · Qiang Li^{3,4} · Xiao Li^{3,4} · Yang Li^{3,4} · Jie Liu⁹ · Shu-Bin Liu^{1,6} · Ze Long^{3,4} · Guang-Yuan Luan⁷ · Chang-Jun Ning^{3,4} · Meng-Chen Niu^{3,4} · Bin-Bin Qi^{1,6} · Jie Ren⁷ · Xi-Chao Ruan⁷ · Zhao-Hui Song¹¹ · Kang Sun^{3,4,12} · Zhi-Jia Sun^{3,4,10} · Zhi-Xin Tan^{3,4} · Jing-Yu Tang^{6,8} · Xin-Yi Tang^{1,6} · Bin-Bin Tian^{3,4} · Li-Jiao Wang^{3,4,12} · Peng-Cheng Wang^{3,4} · Zhao-Hui Wang⁷ · Xiao-Guang Wu⁷ · Xuan Wu^{3,4} · Li-Kun Xie^{6,13} · Xiao-Yun Yang^{3,4} · Li Yu^{3,4} · Tao Yu^{1,6} · Yong-Ji Yu^{3,4} · Guo-Hui Zhang⁹ · Lin-Hao Zhang^{3,4,12} · Qi-Wei Zhang⁷ · Xian-Peng Zhang¹¹ · Yu-Liang Zhang^{3,4} · Zhi-Yong Zhang^{1,6} · Lu-Ping Zhou^{3,4,12} · Zhi-Hao Zhou^{3,4,12} · Ke-Jun Zhu^{3,10,12}

Received: 16 March 2023 / Revised: 6 May 2023 / Accepted: 30 May 2023 / Published online: 16 August 2023

© The Author(s), under exclusive licence to China Science Publishing & Media Ltd. (Science Press), Shanghai Institute of Applied Physics, the Chinese Academy of Sciences, Chinese Nuclear Society 2023

Abstract

The $^{232}\text{Th}(n,f)$ cross section is very important in basic nuclear physics and applications based on the Th/U fuel cycle. Using the time-of-flight method and a multi-cell fast-fission ionization chamber, a novel measurement of the $^{232}\text{Th}(n,f)$ cross section relative to ^{235}U in the 1–200 MeV range was performed at the China Spallation Neutron Source Back-n white neutron source (Back-n). The fission event-neutron energy spectra of ^{232}Th and ^{235}U fission cells were measured in the single-bunch mode. Corrected $^{232}\text{Th}/^{235}\text{U}$ fission cross-sectional ratios were obtained, and the measurement uncertainties were 2.5–3.7% for energies in the 2–20 MeV range and 3.6–6.2% for energies in the 20–200 MeV range. The $^{232}\text{Th}(n,f)$ cross section was obtained by introducing the standard cross section of $^{235}\text{U}(n,f)$. The results were compared with those of previous theoretical calculations, measurements, and evaluations. The measured ^{232}Th fission cross section agreed with the main evaluation results in terms of the experimental uncertainty, and ^{232}Th fission resonances were observed in the 1–3 MeV range. The present results provide $^{232}\text{Th}(n,f)$ cross-sectional data for the evaluation and design of Th/U cycle nuclear systems.

Keywords $^{232}\text{Th}(n,f)$ cross section · Fast-fission ionization chamber · Back-n white neutron source

1 Introduction

Data on neutron-induced fission reactions are important in basic and applied nuclear physics [1]. In a “generation IV” nuclear reactor and accelerator-driven system (ADS), a novel ^{232}Th -based fuel cycle has been proposed for improving the

efficiency and safety of nuclear reactors as well as for transmuting nuclear waste, such as liquid fueled thorium molten salt reactor [2] and thorium-based molten salt fast energy amplifier [3]. In these systems, ^{232}Th is converted to fissile ^{233}U after a neutron capture reaction and two β^- decays [4], partially accounting for the emerging fission. Near the fission threshold, ^{232}Th plays a significant role in neutron delay, contributing up to 2%. In Th/U cycle-based nuclear systems, the $^{232}\text{Th}(n,f)$ cross section should have up to 5% of uncertainty [5].

In addition to its important applications in nuclear systems, the $^{232}\text{Th}(n,f)$ reaction is interesting owing to the

This work was supported by the National Natural Science Foundation of China (Nos. 11675155, 11790321, and 12075216) and the National Key Research and Development Plan (No. 2016YFA0401603).

Extended author information available on the last page of the article

“thorium anomaly” [6, 7]. Möller and Nix [8] explained this phenomenon using a triple-humped barrier, owing to the difficulty associated with describing the structure using a double-humped barrier. By studying the resonances in the $^{232}\text{Th}(n,f)$ reaction, a profound understanding of the nuclear structure can be achieved. Therefore, it is very important to measure the high-precision $^{232}\text{Th}(n,f)$ cross section in a wide range of energies.

During the last few decades, various measurements of the $^{232}\text{Th}(n,f)$ cross section have been performed. Behrens [9] measured the $^{232}\text{Th}(n,f)$ cross section for energies in the 0.7–30 MeV range, using parallel plate ionization fission chambers and photoneutrons; these measurements were performed at the Lawrence Livermore National Laboratory in 1982. The overall uncertainty associated with that experiment was in the 2.5–61.7% range. In 1983, Meadows et al. [10] measured the $^{232}\text{Th}(n,f)$ cross section with an ionization chamber and monoenergetic neutron flux at Argonne Fast Neutron Generator Laboratory, for energies ranging from 1.2 to 9.9 MeV; the uncertainty was in the 1.5–10.8% range. In 1988, Lisowski et al. [11] measured the cross-sectional ratio $^{232}\text{Th}/^{235}\text{U}(n,f)$ for energies in the 1–400 MeV range, using a multiple-plate gas ionization chamber at the Weapons Neutron Research Facility at Los Alamos National Laboratory; the uncertainty was in the 1.4–9.1% range. Fursov et al. [12] also measured the cross-sectional ratio for neutrons with energies in the 0.13–7.4 MeV range; the experimental uncertainty ranged from 2.2 to 15%. These measurements were performed using a fission chamber at the electrostatic accelerator at the Power Physics Institute. Using the time-of-flight (TOF) method and fast parallel plate ionization chambers, Shcherbakov et al. [13] measured energies in the 1–200 MeV range in 2002, using the neutron spectrometer GNEIS; the uncertainty was in the 0.5–9.9% range.

Recently, Michalopoulou et al. [7] measured the $^{232}\text{Th}(n,f)$ cross section using micromegas detectors with quasi-monoenergetic neutron beams with energies in the 2–18 MeV range; the uncertainty was in the 1.6–8.0% range. Using d–d neutron sources and back-to-back Th/ ^{238}U samples, Gledenov et al. [14] performed measurements at 12 energy points, for energies ranging from 4.2 to 11.5 MeV; the uncertainty was in the 3.7–5.8% range. These measurements were performed at Peking University and China Institute of Atomic Energy. Chen et al. [15] measured the $^{232}\text{Th}(n,f)$ cross sections relative to the $^{235}\text{U}(n,f)$ cross section and n–p scattering, for energies in the 1–300 MeV range, using a fast-ionization chamber and a proton recoil telescope at the Back-n facility. The measurements were performed in the double-bunch mode at an Endstation 1. The measured results were normalized to the evaluation data at approximately 14 MeV, and the uncertainty was in the 3.9–27.4% range.

The upper limit of the $^{232}\text{Th}(n,f)$ cross section in the ENDF/B-VIII.0 evaluation was 60 MeV, and that obtained in other evaluations was 20 MeV [16–20]. The different evaluations of the $^{232}\text{Th}(n,f)$ cross section exhibit large discrepancies, especially at the fission threshold and high-energy points. For energies up to 20 MeV, the differences reach 10% and are much larger near the threshold. For energies above 20 MeV, only the data of Shcherbakov et al., Lisowski et al., and Chen et al. cover the range of energies up to 200 MeV. However, these datasets for energies above 20 MeV still exhibit significant discrepancies, reaching 30%. These discrepancies create obstacles for applications in both basic and applied nuclear physics.

To provide independent experimental data, a novel measurement of the $^{232}\text{Th}(n,f)$ cross section, for energies in the 1–200 MeV range, was performed at the China Spallation Neutron Source (CSNS) Back-n [21, 22]. A multi-cell fission ionization chamber (MFIC) [23–25] and high-purity thorium and uranium samples were used for these measurements. The experimental method and setup are described in Sects. 2 and 3, respectively. After a detailed introduction to the data analysis in Sect. 4, 5 presents the results and discussion. Finally, Sect. 6 summarizes this study.

2 Experimental method

In this study, the TOF method, relative method, and MFIC were used for measuring the $^{232}\text{Th}(n,f)$ cross section at the CSNS Back-n. The energies of the incident neutrons were obtained using the TOF method, and the neutron flux was canceled out owing to relative measurements. Various fission cells mounted in the chamber were used for measuring the fission signals owing to the different samples.

The $^{235}\text{U}(n,f)$ cross section was used as a neutron standard at 0.0253 eV, 7.8–11 eV, and 0.15–200 MeV, which is fundamental for measurements that use the relative method. The uncertainties of the neutron standards file increased from < 1 to 4.5% for the 0.15–200 MeV range of energies [26]. The $^{232}\text{Th}(n,f)/^{235}\text{U}(n,f)$ cross-sectional ratios were determined using Eq. (1).

$$\frac{\sigma_{232\text{Th}}}{\sigma_{235\text{U}}} = \frac{N_{\text{FF } 232\text{Th}}}{N_{\text{FF } 235\text{U}}} \cdot \frac{\varepsilon_{235\text{U}}}{\varepsilon_{232\text{Th}}} \cdot \frac{N_{235\text{U}}}{N_{232\text{Th}}} \cdot \frac{A_{235\text{U}}}{A_{232\text{Th}}} \cdot \frac{Q_{235\text{U}}}{Q_{232\text{Th}}} \cdot \frac{\eta_{232\text{Th}}}{\eta_{235\text{U}}}, \quad (1)$$

where σ is the cross section, and N_{FF} is the number of fission events measured by the MFIC. In addition, ε is the detection efficiency of each fission cell calculated using the amplitude spectra. N is the number of atoms in each fission sample with an approximate uncertainty of 1%. A , Q , and η account for the neutron flux attenuation, nonuniformity, and sample contamination correction, respectively, of each cell.

3 Experimental setup

3.1 Back-n white neutron source

At the Back-n white neutron source [21, 22], 1.6-GeV-energy protons were projected onto a tungsten target, and neutrons with different energies were emitted in all directions via the spallation reaction. The measurements were performed in the single-bunch mode for 12 h. The power of the proton beam was 40 kW, and the frequency was 25 Hz. The detector was set in the neutron beam at Endstation 2 of Back-n. The neutron beam spot at Endstation 2 had $\Phi=60$ mm and the full width at half maximum (FWHM) of each neutron bunch was approximately 60 ns. The neutron beam had approximately 2.81×10^6 n/cm²/s at Endstation 2 with water serving as a coolant passing through the thick tungsten target, yielding an excellent wide-energy-spectrum distribution, with energies ranging from 1 eV to 200 MeV [27]. In these measurements, thermal neutrons were absorbed by a 1-mm-thick Cd foil.

3.2 MFIC

Based on a previously described fission ionization chamber [23–25], a detection system was developed at Back-n, consisting of an MFIC with a faster response time, associated electronics, and a data acquisition and processing system [21].

The MFIC was carefully optimized, as follows. The stainless-steel cylindrical shell of the MFIC was replaced with an aluminum shell. The neutron beam window, gas interfaces, and cable connectors were optimized in terms of their structure and material. The improved chamber was lighter, more versatile, and had less electromagnetic noise. The structure of each fission cell was modified to reduce the capacitance between the electrodes. Simultaneously, the chamber was filled with the P10 gas (90% Ar and 10% CF₄) at approximately 0.8 bar. Changes in the structure and working gas led to a fast response time (less than 30 ns).

The MSI-8 preamplifier was chosen for the multi-cell fast-fission ionization chamber owing to its large amplification, fast response, and low output noise. The preamplifier signals were digitized using the Back-n data acquisition (DAQ) system [28]. Figure 1 shows the optimized MFIC for Endstation 2.

3.3 Samples

For the measurements, three ^{232}Th and two ^{235}U high-purity fission samples were used: ^{235}U -1, ^{235}U -5, ^{232}Th -1, ^{232}Th -2, and ^{232}Th -3. These fission nuclides were electroplated on

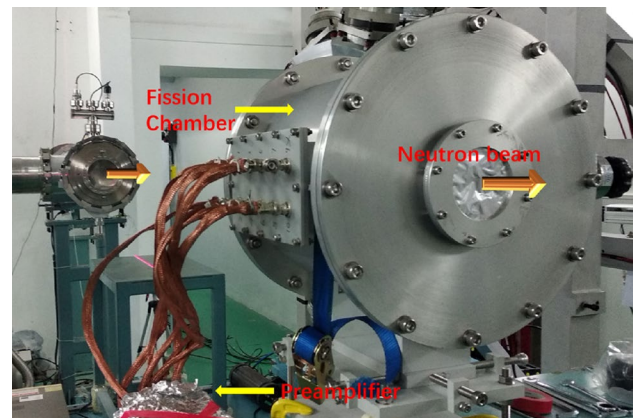


Fig. 1 Optimized MFIC mounted at Endstation 2 in the present study

the backings of aluminum steel or stainless (^{235}U -1) in the form of U_3O_8 and ThO_2 . The diameters of the backing and deposit were 80 mm and 50 mm, respectively. The masses of the samples were determined from their spontaneous-decay alpha-particle spectra, which were measured using a small solid-angle physical quantitative counting device [29]. The quality uncertainty ranges of the samples were calculated using an error propagation formula. Figure 2 shows the measured particle spectrum of the ^{232}Th -1 sample. The characteristics of the different fission samples along the neutron beam used in this study are listed in Table 1. The abundance of impurities of the ^{232}Th sample was less than 10^{-6} ; thus, it was ignored.

The ^{232}Th samples were assumed to be 100% abundant, and the ^{235}U samples were enriched to 99.985% [30]. The mass distributions of the fission samples were obtained using an α -sensitive imaging plate placed over the surfaces of the samples. The ^{232}Th sample and its mass distribution with 0.2 mm \times 0.2 mm pixels are shown in Fig. 3. Darker colors indicate more nuclides. Mass distribution images were used for the uniformity determination and correction of the studied samples.

4 Data analysis

4.1 Processing of raw data

When a neutron bunch was produced by the CSNS, a synchronous signal T_0 triggered the DAQ system, and all signals exceeding the threshold within 10 ms were collected. The experimental data were recorded as 0.5 TB-size raw files in the form of packets, including the information about the signal waveform and channel number. The original raw files were processed using various C++ programs based on ROOT [31]. Figure 4 shows the signal

Fig. 2 α -particle spectrum of the ^{232}Th sample. The α decay chain of the ^{232}Th sample is clearly seen

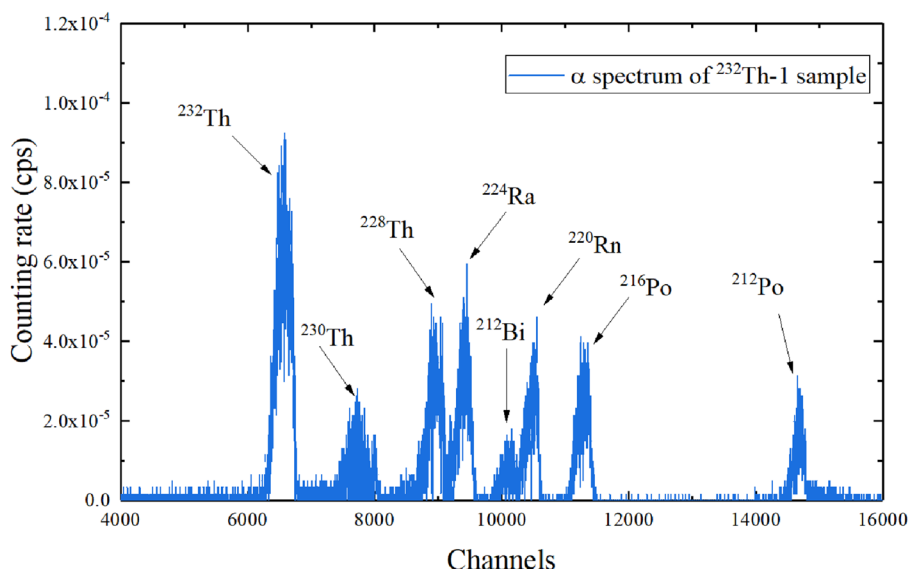


Table 1 Characteristics of the fission samples along the neutron beam used in the present work

Sample	Mass (mg)	Uncertainty (%)	Diameter (cm)	Mass thickness (mg/cm ²)	Non-uniformity (%)
^{235}U -1	5.173	1.0	4.974	0.266	9.6
^{235}U -5	6.319	0.9	4.976	0.293	8.6
^{232}Th -1	3.477	1.2	4.969	0.177	11.2
^{232}Th -2	3.207	1.3	4.972	0.163	13.7
^{232}Th -3	3.372	1.3	4.971	0.172	14.1
Al	–	–	–	–	–

4.2 Amplitude spectrum

The signals of fission, γ -flash, α -particle, and electronic noise were recorded using the DAQ system. The fast-fission ionization chamber was insensitive to γ signals. Therefore, only γ -flash could be detected. Figure 5 shows the amplitude spectra of the ^{235}U and ^{232}Th fission cells and the Al cell (background), measured using the MFIC within the neutron beam. In this figure, the background is mainly attributed to the α decay of the fissile isotopes and (n,lcp) reactions of the sample backing and the aluminum collector.

As shown in Fig. 5, the background is distributed in the low-amplitude region. In addition, the fission signals are distributed throughout the observed region. Therefore, amplitude thresholds were set for each fission cell to distinguish fission signals from other noise. The amplitude thresholds for ^{235}U and ^{232}Th cells are marked with blue dotted lines. The signals of the fission cells are shown as colored solid lines and are widely distributed. The background signal (red solid line) is mainly below the amplitude thresholds, and the few events above the threshold can be neglected.

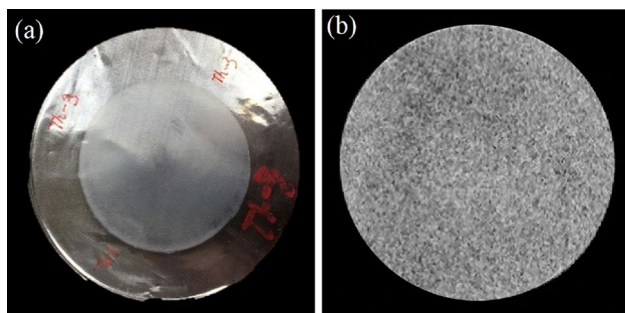


Fig. 3 ^{232}Th sample (a) and its mass distribution (b)

waveform measured for the ^{232}Th fission cell. Contrastingly, the amplitudes of the different signals were recorded for obtaining the amplitude spectra, which were used for distinguishing fission signals from other signals. Furthermore, the time difference between the fission and γ -flash signals was used for computing the flight time of the neutrons that induced this fission event.

4.3 Detection efficiency

The MFIC detection efficiency ϵ can be calculated using Eq. (2) [32]. Fission events are primarily lost owing to self-absorption and amplitude threshold settings, which correspond to the first and second terms in the below equation:

$$\epsilon = \left(1 - \frac{t}{2R}\right) \times \left(1 - \frac{N_L}{N_U}\right). \tag{2}$$

Fig. 4 A typical signal waveform measured for the ^{232}Th fission cell. The horizontal coordinate is the time information about the waveform, while the vertical coordinate captures the signal amplitude. The 10–90% temporal window of the rising edge was approximately 30 ns

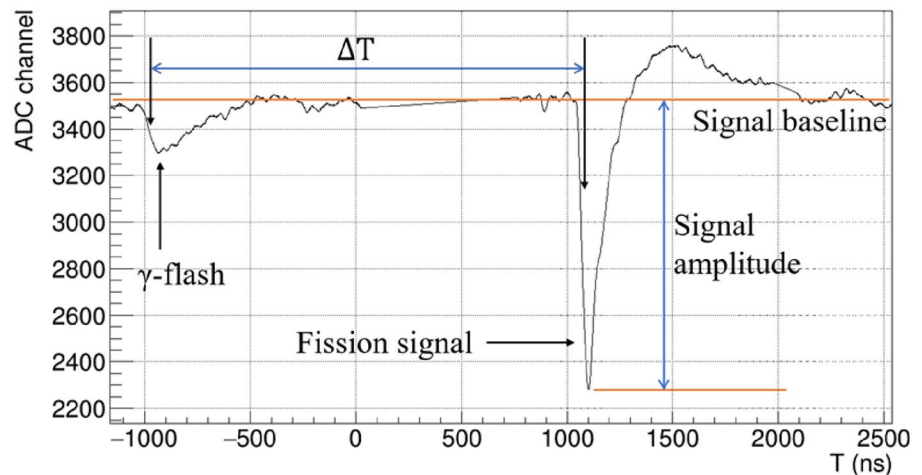
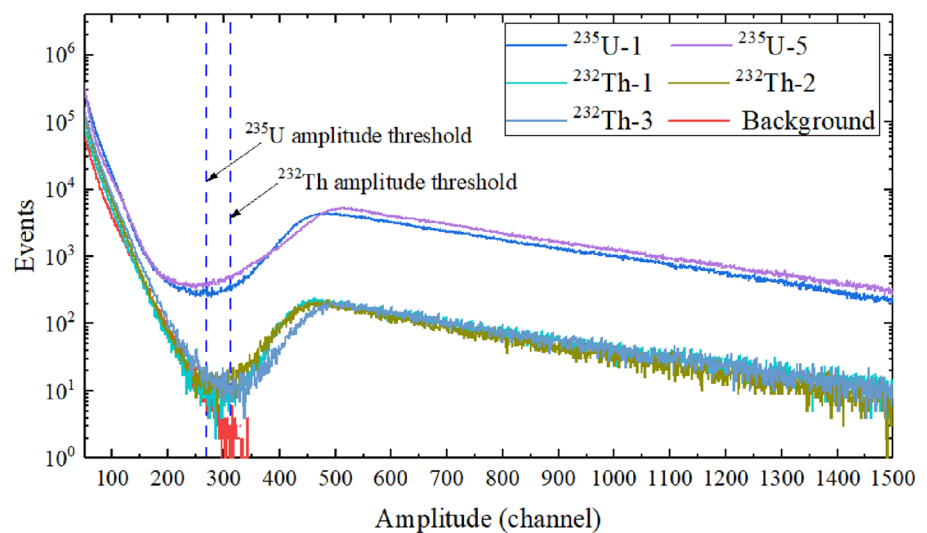


Fig. 5 (Color online) Amplitude spectra of the ^{235}U , ^{232}Th fission cells and Al cell (background), measured using the MFIC. The amplitude thresholds were set for different fission cells to distinguish the fission signals from other noise sources



The average ranges of fission fragments (R) for the U_3O_8 and ThO_2 deposits were $7.5 \pm 0.5 \text{ mg/cm}^2$ [33] and $8.0 \pm 0.5 \text{ mg/cm}^2$, respectively. The R value for ThO_2 was calculated using the approach described in Ref. [32], where N_L and N_U represent the counts of fission events below and above the amplitude threshold, respectively. To calculate N_L , a constant number was assumed using the “flat tail” assumption below the amplitude threshold.

The efficiencies of the two ^{235}U and three ^{232}Th fission cells were 94.90%, 94.65%, 95.94%, 95.68%, and 96.00%, respectively. The detection efficiencies with respect to different energy regions were analyzed and found to change weakly [34]. The uncertainties of the efficiencies of the ^{235}U and ^{232}Th fission cells were 0.2–0.3% and 0.2–0.4%, respectively, mainly owing to the statistical uncertainty of N_L .

4.4 Energy calibration

The neutron TOF_n was calculated using Eq. (3) [30]:

$$\text{TOF}_n = T_f - T_n = T_f - T_\gamma + \text{TOF}_\gamma. \quad (3)$$

In the above equation, T_f and T_γ are the detected time of the fission signal and γ -flash recorded using the MFIC detector; T_n is the production time of neutrons; and TOF_γ is the TOF of the γ -flash. In fact, the uncertainty of T_n was 60 ns, owing to the FWHM of each neutron bunch. The TOF_γ value was inferred from the determined flight distance. The T_f and T_γ values were well determined in the 0.4 constant fraction timing point (40% of the rising edge of signals).

Many γ -flash signals were used for yielding a standardized γ -flash waveform. The T_γ calibration results for the two ^{235}U cells and three ^{232}Th cells were -969 ns , -999 ns , -1000 ns , -999 ns , and -1000 ns . The averaged γ -flash waveform measured for the ^{235}U -1 cell is shown in Fig. 6a.

TOF_γ was calculated by dividing the accurate flight distance by the speed of light. The 8.77-eV-energy resonance peak of the $^{235}\text{U}(n,f)$ reaction was chosen for the flight distance calculation, as shown in Fig. 6b. A detailed description

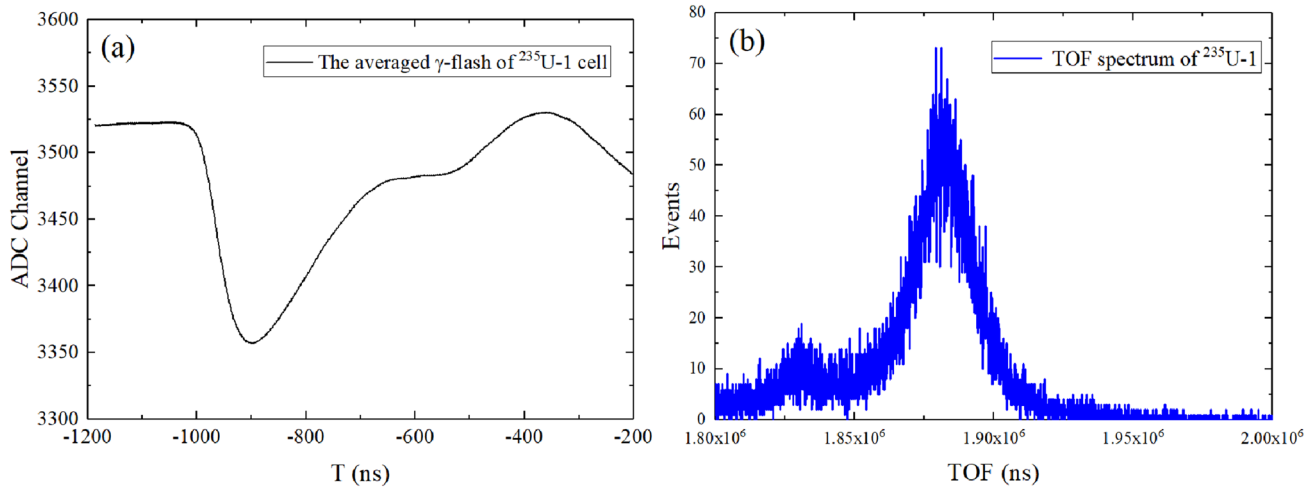


Fig. 6 Averaged γ -flash waveform (a) and the TOF spectrum of the 8.77-eV-energy resonance peak (b) measured for the ^{235}U -1 fission cell

of the flight distance determination can be found in Ref. [30]. The estimated flight distance for the ^{235}U -1 fission cell was 77.073 m, and the positioning uncertainty was 3 mm. The flight distances for the other fission cells were obtained using the geometric dimensions of the MFIC.

4.5 Fission event-neutron energy spectra

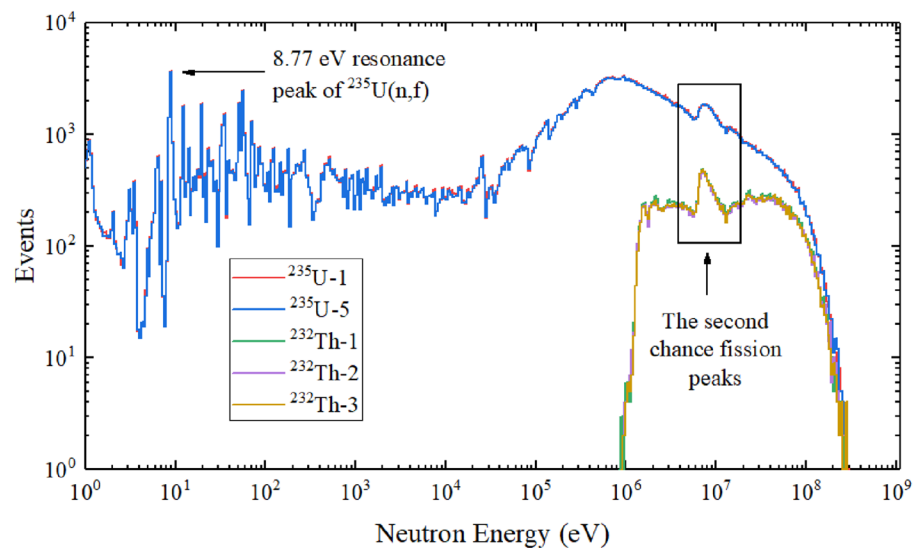
Figure 7 shows the fission event-neutron energy spectra obtained for the ^{235}U and ^{232}Th fission cells, with the preliminary results divided into 100 bins per decade. The resonance peaks attributed to the $^{235}\text{U}(n,f)$ reaction are clearly observed in the 1–1000 eV range. The distribution of second-chance fission is also observed for energies in the 6–8 MeV range. In the ^{232}Th spectrum, there are fewer fission events below 1 MeV, owing to the fission threshold at

1.3 MeV. As shown in Fig. 7, the two ^{235}U spectra and three ^{232}Th datasets (normalized with mass) are concordant. These observations validate the reliability of our measurements.

4.6 Corrections

In the present experiments, the fast-ionization chamber contained various fission cells in the direction of the incident neutrons. The neutron flux gradually attenuated as it passed through the fission cells of the MFIC, owing to interactions with the backing and collectors. A Monte Carlo simulation [35] was used to assess the flux attenuation in different fission cells based on the geometric design of the detector and fission samples. The simulation results showed that the neutron flux decreased as the number of cells increased. In the last ^{232}Th -3 cell, the neutron flux attenuation was 1.0–2.5%,

Fig. 7 (Color online) Measured fission event-neutron energy spectra, shown on the log–log scale



for energies in the 1–200 MeV range; the uncertainty was in the 0.2–2% range.

The nonuniformities of the ^{235}U and ^{232}Th samples obtained with α -sensitive imaging plates are listed in Table 1 and that of the neutron beam was obtained from simulations. The nonuniformity correction factor is described in detail in Ref. [36]. The correction factors for the ^{232}Th and ^{235}U samples were 1.0023–1.0028 and 1.0026–1.0046, respectively. The uncertainty of the Q values was approximately 0.1%.

The dead time was negligible because the signal counting rate ($1.2 \times 10^3/\text{s}$) was much lower than the DAQ acquisition rate, and the frame overlap probability of each independent channel was below 10^{-5} . In addition, the samples were corrected for impurities, based on the abundance of isotopes and their fission cross sections. The ^{232}Th sample was assumed to be 100% abundant, and the correction factor was 1. In addition, in the 1–200 MeV range, the correction factor of the ^{235}U sample was 0.99988–0.99999; the associated uncertainty was less than 0.01%, allowing to neglect the correction.

5 Results and discussion

5.1 $^{232}\text{Th}/^{235}\text{U}(n,f)$ cross-sectional ratio

The $^{232}\text{Th}/^{235}\text{U}(n,f)$ cross-sectional ratio for energies in the 1–200 MeV range was obtained in the single-bunch mode, according to Eq. (1). Six datasets were obtained using two ^{235}U and three ^{232}Th fission cells were used for obtaining averages. As shown in Fig. 8, the experimental data were compared with those of previous experiments, and the ratio was extracted from the ENDF/B-VIII.0 evaluation [16]. The average discrepancies between these data and the ENDF/B-VIII.0 [16] data were -1.0 – 2.5% for energies in

Fig. 8 (Color online) Comparison of the measured data with previously reported experimental data, for energies in the 1–200 MeV range [9–13, 16]

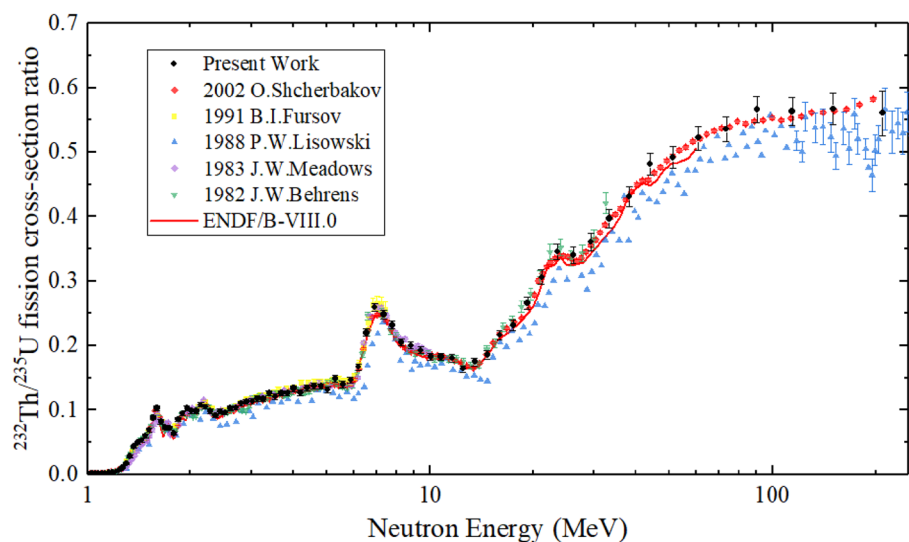


Table 2 Uncertainties of the measured ratios

Content	^{235}U cell (%)	^{232}Th cell (%)
N_{ff}	0.6–0.8 (1–20 MeV)	3.1–33.3 (1–2 MeV)
	0.7–2.6 (20–210 MeV)	1.6–3.1 (2–20 MeV)
		1.4–4.6 (20–210 MeV)
N	0.9–1.0	1.2–1.3
A	0.2–2.0	0.2–2.0
ε	0.2–0.3	0.2–0.4
Q	0.1	0.1
η	< 0.01	–
Total	3.5–33.4 (1–2 MeV)	
	2.5–3.7 (2–20 MeV)	
	3.6–6.2 (20–210 MeV)	

the 2–60 MeV range. The average discrepancy between the final average ratio and that of ENDF/B-VIII.0 was 0.8% for energies in the 2–60 MeV range, confirming the accuracy of the ENDF/B-VIII.0 evaluation. The energy resolution of this measurement varied from 1.6 to 27% for energies in the 1–200 MeV, which was the same as that described in detail in Refs. [30, 37]. To match the energy resolution, the data in this region were divided into 86 bins, and the energy point was the center point of the corresponding bin.

The comparison indicates a good agreement between the results obtained in the present study and those obtained using the ENDF/B-VIII.0 evaluation. The ratio measured in this experiment was consistent with that reported by Shcherbakov et al. [13] for energies in the 1–200 MeV range and agreed well with the results reported by Behrens [9], Meadows [10], and Fursov [12] within the reported uncertainties. In addition, the data reported by Lisowski et al. [11] were lower than those reported by the other groups.

Table 2 lists the measurement uncertainties of the reported ratio values. The measurement uncertainties were

mainly derived from statistical and quantification uncertainties. The fission threshold of the $^{232}\text{Th}(n,f)$ reaction and the decrease in the neutron flux for energies above 20 MeV increased the statistical uncertainty in the corresponding region. The 210 MeV-energy points in Table 2 represent the bins for energies in the 172–248 MeV range.

5.2 $^{232}\text{Th}(n,f)$ cross section

The neutron-induced ^{232}Th fission cross section was obtained along with the $^{235}\text{U}(n,f)$ cross section [26] and the measured ratio, as explained in Sect. 5.1. The experimental uncertainties were 2.9–4.0% for energies in the 2–20 MeV range and 4.0–7.7% for energies in the 20–200 MeV range, respectively. The calculation program UNF [38] was used to calculate the theoretical results for energies in the 1–20 MeV range. Several theoretical models have been used to calculate

the reaction processes and different cross sections. The specific process of theoretical calculations is described in Ref. [30].

Figure 9 compares the $^{232}\text{Th}(n,f)$ cross-sectional measurements of the current study with those reported by previous studies. Figure 10 compares the measured data with the calculated and evaluated data. Figure 11 compares the results for the 1–7 MeV range of energies. The experimental results of the present study agreed with the data of Shcherbakov et al. [13] and Chen et al. [15] for energies in the 1–200 MeV range; the values were within the range of experimental uncertainties. The measured cross section agreed with the calculation and main evaluation results, except for a large discrepancy with the ADS-HE evaluation for energies exceeding 60 MeV, as shown in Fig. 11. For energies in the 1–7 MeV range, the data obtained in this study were concordant with those reported by Gledenov et al. [14], which

Fig. 9 (Color online) Comparison of the measured $^{232}\text{Th}(n,f)$ cross section with those reported by previous studies [7, 10, 11, 13–15]

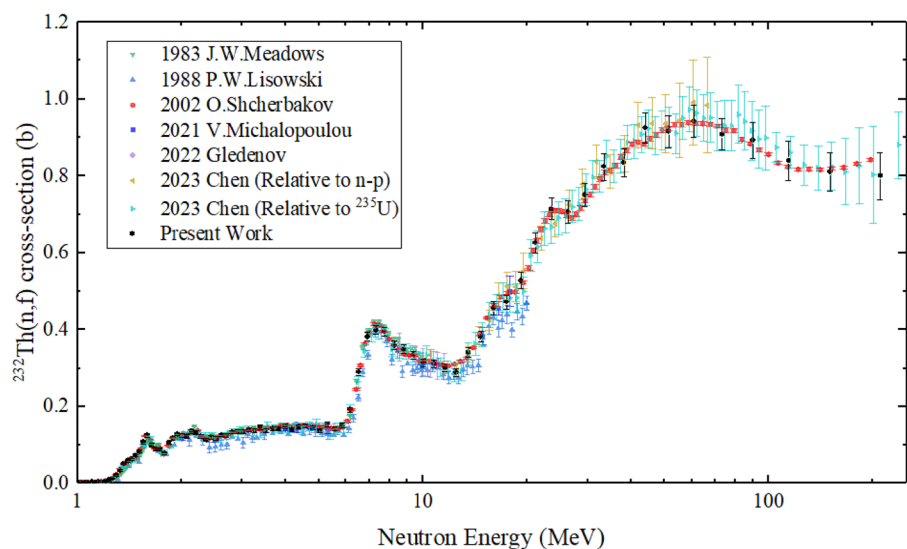


Fig. 10 (Color online) Comparison of the measured $^{232}\text{Th}(n,f)$ cross section with previously calculated and evaluated data [16–19, 39]

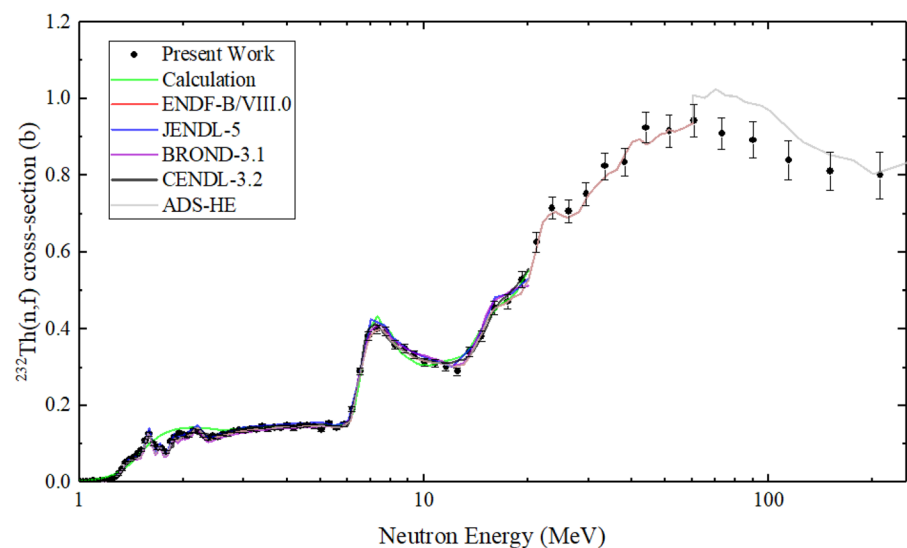
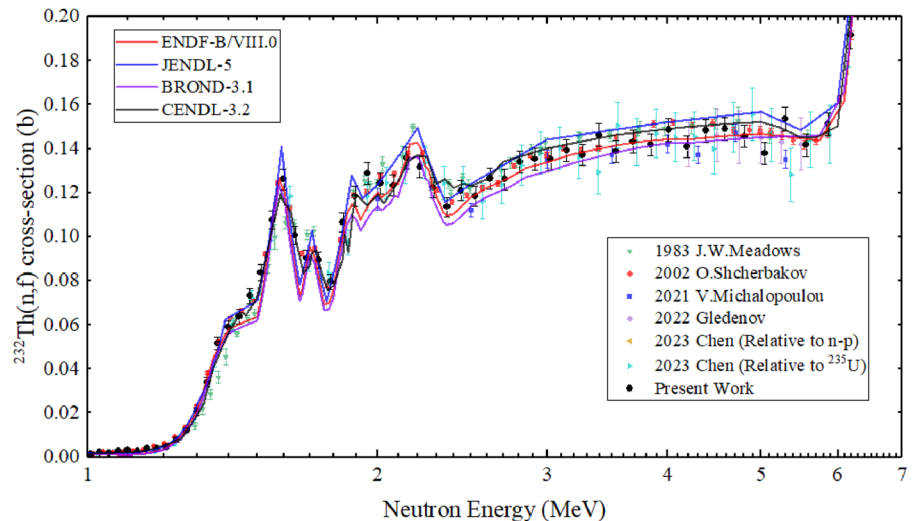


Fig. 11 (Color online) Comparison of the measured $^{232}\text{Th}(n,f)$ cross section with previous results, calculations, and main evaluations, for energies in the 1–7 MeV range; the results are shown on the logarithmic scale [7, 10, 13–19]



in turn were slightly lower than those reported by Meadows et al. [10] and higher than those reported by Michalopoulou et al. [7], as shown in Fig. 11. The resonances of the $^{232}\text{Th}(n,f)$ reaction for energies in the 1–3 MeV range (thorium anomaly behavior) were observed in the present measurements and were consistent with previously reported results and evaluations, within the experimental uncertainty.

Figure 12 shows the ratios of the measured data to the calculation results and main evaluations. The average discrepancies between the measured data and corresponding

evaluations were -0.77% , 4.13% , -1.36% , 1.91% , and -0.77% for energies in the 2–20 MeV range. Evidently, there are large discrepancies for energies in the 1–2 MeV range. In the UNF calculation, a large discrepancy was observed for energies in the 1–3 MeV range, owing to the “thorium anomaly”. For most of the evaluated energy points, the results obtained in the present study agree with the ENDF/B-VIII.0 evaluation results more than with other evaluation results. For energies higher than 60 MeV, there is a sudden increase in the ^{232}Th fission cross section in the

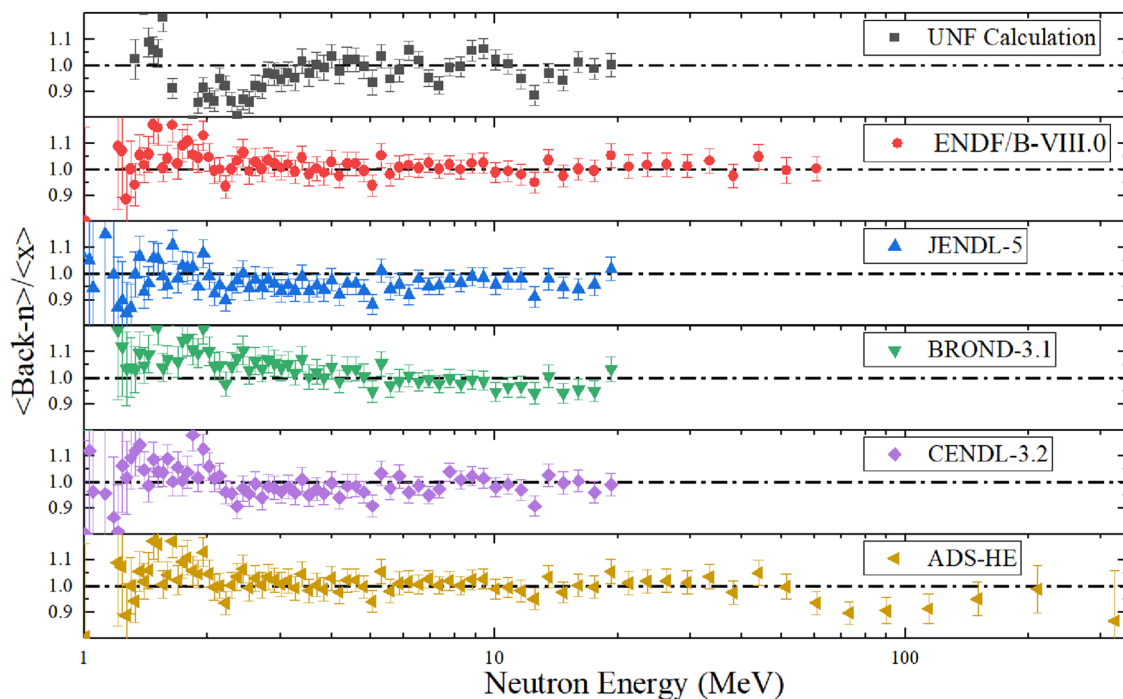


Fig. 12 (Color online) Ratios of the data measured in this study to calculated and evaluated data [16–19, 39]

ADS-HE database, which was not observed in the present work.

6 Conclusion

The $^{232}\text{Th}(n,f)$ fission cross section, for energies ranging from 1 to 200 MeV, was measured relative to ^{235}U in the single-bunch mode at the CSNS Back-n. An MFIC with five high-purity fission samples was used in these measurements. In the energy calibration, the TOF of the neutrons was calculated using the fission and γ -flash signals. After the calibration of the detection efficiency and corrections of various influencing factors, absolute $^{232}\text{Th}/^{235}\text{U}(n,f)$ cross-sectional ratios were obtained for energies in the 1–200 MeV range, with the experimental uncertainty of 2.5–3.7% for energies in the 2–20 MeV range and 3.6–6.2% for energies in the 20–200 MeV range. The $^{232}\text{Th}(n,f)$ cross section was obtained by introducing the standard $^{235}\text{U}(n,f)$ cross section. Resonances of the $^{232}\text{Th}(n,f)$ reaction for energies in the 1–3 MeV range were observed and were consistent with those of previous experiments and evaluations.

The measured data were more consistent with the ENDF/B-VIII.0 evaluation than other evaluations. The data of the present experiment are in agreement with the data of Shcherbakov et al. [13] and Chen et al. [15] for energies in the 1–200 MeV range, within a range of experimental uncertainties. The data also exhibit the same trends as the theoretical results obtained using the UNF code. These novel measurements can provide experimental data for addressing the discrepancies among main evaluations. Specifically, for energies above 20 MeV, the measured data of the present study are important for improving evaluations, owing to the data paucity for energies in that range.

Author contributions All authors contributed to the study conception and design. Material preparation, data collection, and analysis were performed by Zhi-Zhou Ren, Yi-Wei Yang, Yong-Hao Chen, Rong Liu, Bang-Jiao Ye, Jie Wen, Hai-Rui Guo, Zi-Jie Han, Qi-Ping Chen, Zhong-Wei Wen, Wei-Li Sun, Han Yi, Xing-Yan Liu, Tao Ye, Jiang-Bo Bai, Qi An, Jie Bao, Yu Bao, Ping Cao, Hao-Lei Chen, Zhen Chen, Zeng-Qi Cui, Rui-Rui Fan, Chang-Qing Feng, Ke-Qing Gao, Xiao-Long Gao, Min-Hao Gu, Chang-Cai Han, Guo-Zhu He, Yong-Cheng He, Yang Hong, Yi-Wei Hu, Han-Xiong Huang, Xi-Ru Huang, Hao-Yu Jiang, Wei Jiang, Zhi-Jie Jiang, Han-Tao Jing, Ling Kang, Bo Li, Chao Li, Jia-Wen Li, Qiang Li, Xiao Li, Yang Li, Jie Liu, Shu-Bin Liu, Ze Long, Guang-Yuan Luan, Chang-Jun Ning, Meng-Chen Niu, Bin-Bin Qi, Jie Ren, Xi-Chao Ruan, Zhao-Hui Song, Kang Sun, Zhi-Jia Sun, Zhi-Xin Tan, Jing-Yu Tang, Xin-Yi Tang, Bin-Bin Tian, Li-Jiao Wang, Peng-Cheng Wang, Zhao-Hui Wang, Xiao-Guang Wu, Xuan Wu, Li-Kun Xie, Xiao-Yun Yang, Li Yu, Tao Yu, Yong-Ji Yu, Guo-Hui Zhang, Lin-Hao Zhang, Qi-Wei Zhang, Xian-Peng Zhang, Yu-Liang Zhang, Zhi-Yong Zhang, Lu-Ping Zhou, Zhi-Hao Zhou, and Ke-Jun Zhu. The first draft of the manuscript was written by Zhi-Zhou Ren, and all authors commented on previous versions of the manuscript. All authors read and approved the final manuscript.

Data availability The data that support the findings of this study are openly available in Science Data Bank at <https://www.doi.org/10.57760/sciencedb.09535> and <https://cstr.cn/31253.11.sciencedb.09535>.

Declarations

Conflict of interest Jing-Yu Tang, Ke-Jun Zhu, and Chang-Qing Feng are editorial board members for Nuclear Science and Techniques and were not involved in the editorial review, or the decision to publish this article. All authors declare that there are no competing interests.

References

1. N. Colonna, A. Tsinganis, R. Vlastou et al., The fission experimental programme at the CERN n_TOF facility: status and perspectives. *Eur. Phys. J. A* **56**, 48 (2020). <https://doi.org/10.1140/epja/s10050-020-00037-8>
2. C.Y. Li, X.B. Xia, J. Cai et al., Radiation dose distribution of liquid fueled thorium molten salt reactor. *Nucl. Sci. Tech.* **32**, 22 (2021). <https://doi.org/10.1007/s41365-021-00857-3>
3. P. Yang, Z.K. Lin, W.S. Wan et al., Preliminary neutron study of a thorium-based molten salt energy amplifier. *Nucl. Sci. Tech.* **31**, 41 (2020). <https://doi.org/10.1007/s41365-020-0750-8>
4. International Atomic Energy Agency (IAEA), Thorium fuel cycle—potential benefits and challenges. (IAEA-TEC-DOC-1450, 2005), Accessed 19 Jul 2021. <https://www.iaea.org/publications/7192>
5. U. Abbondanno, S. Andriamonje, J. Andrzejewski et al., Measurements of fission cross sections for the isotopes relevant to the thorium fuel cycle. CERN/INTC 2001–25, 08 Aug 2001. <https://cds.cern.ch/record/514756/files/intc-p-145.pdf>
6. S. Bjørnholm, J.E. Lynn, The double-humped fission barrier. *Rev. Mod. Phys.* **52**, 725 (1980). <https://doi.org/10.1103/RevModPhys.52.725>
7. V. Michalopoulou, M. Axiotis, S. Chasapoglou et al., Measurement of the $^{232}\text{Th}(n, f)$ cross section with quasi-monoenergetic neutron beams in the energy range 2–18 MeV. *Eur. Phys. J. A* **57**, 277 (2021). <https://doi.org/10.1140/epja/s10050-021-00590-w>
8. P. Möller, J. Nix., Calculation of Fission Barriers, in *Proceedings of the Third IAEA symposium on the physics and chemistry of fission* (Rochester, New York, 1974), p. 103. <https://www.osti.gov/biblio/4458292/>
9. J.W. Behrens, J.C. Browne, E. Ables, Measurement of the neutron-induced fission cross section of ^{232}Th relative to ^{235}U from 0.7 to 30 MeV. *Nucl. Sci. Eng.* **81**(4), 512–519 (1982). <https://doi.org/10.13182/NSE82-A21440>
10. J.W. Meadows., The fission cross sections of some thorium, uranium, neptunium and plutonium isotopes relative to ^{235}U . *Techn. Rep. No. ANL/NDM-83* (1983). <https://doi.org/10.2172/5539010>
11. P.W. Lisowski, J.L. Ullman, S.J. Balestrini et al., Neutron induced fission cross section ratios for ^{232}Th , $^{235,238}\text{U}$, ^{237}Np and ^{239}Pu from 1 to 400 MeV. in *Conference. on Nuclear data for science and technology* p. 97 (1988). <https://www.osti.gov/biblio/6967752>
12. B.I. Fursov, EYu. Baranov, M.P. Klemyshev et al., Measurements of the fission cross-section ratios $^{232}\text{Th}/^{235}\text{U}$ and $^{234}\text{U}/^{235}\text{U}$ for 0.13–7.4 MeV neutrons. *At. Energiya* **71**(4), 827–831 (1991). <https://doi.org/10.1007/BF01123535>
13. O. Shcherbakov, A. Donets, A. Evdokimov et al., Neutron-induced fission of ^{233}U , ^{238}U , ^{232}Th , ^{239}Pu , ^{237}Np , ^{nat}Pb and ^{209}Bi relative to ^{235}U in the energy range 1–200 MeV. *Nucl. Sci. Technol.* **39**, 230 (2002). <https://doi.org/10.1080/00223131.2002.10875081>

14. Y.M. Gledenov, Z.Q. Cui, J. Liu et al., Cross section of the $^{232}\text{Th}(n, f)$ reaction in the MeV neutron energy region. *Eur. Phys. J. A* **58**, 86 (2022). <https://doi.org/10.1140/epja/s10050-022-00716-8>
15. Y.H. Chen, Y.W. Yang, Z.Z. Ren et al., Measurement of neutron-induced fission cross sections of ^{232}Th from 1 to 300 MeV at CSNS Back-n. *Phys. Lett. B* **839**, 137832 (2023). <https://doi.org/10.1016/j.physletb.2023.137832>
16. D.A. Brown, M.B. Chadwick, R. Capote et al., ENDF/B-VIII.0: The 8th major release of the nuclear reaction data library with CIELO-project cross sections, new standards and thermal scattering data. *Nucl. Data Sheets* **148**, 1–142 (2018). <https://doi.org/10.1016/j.nds.2018.02.001>
17. O. Iwamoto, N. Iwamoto, K. Shibata et al., Status of JENDL. In *EPJ Web of conferences*, vol. 239, (2020), p. 09002. <https://doi.org/10.1051/epjconf/2F202023909002>
18. Z.G. Ge, R.R. Xu, H.C. Wu et al., CENDL-3.2: The new version of Chinese general purpose evaluated nuclear data library. *EPJ Web. Conf.* **239**, 09001 (2020). <https://doi.org/10.1051/epjconf/202023909001>
19. A.I. Blokhin, E.V. Gai, A.V. Ignatyuk et al., New version of neutron evaluated data library BROND-31. *Yad. Reak. Konst.* **2**, 62 (2016)
20. A. Plompen, O. Cabellos, C. De SaintJean et al., The joint evaluated fission and fusion nuclear data library, JEFF-33. *Eur. Phys. J. A* **56**, 181 (2020). <https://doi.org/10.1140/epja/s10050-020-00141-9>
21. J.Y. Tang, Q. An, J.B. Bai et al., Back-n white neutron source at CSNS and its applications. *Nucl. Sci. Tech.* **32**, 11 (2021). <https://doi.org/10.1007/s41365-021-00846-6>
22. H.T. Jing, J.Y. Tang, H.Q. Tang et al., Studies of back-streaming white neutrons at CSNS. *Nucl. Instrum. Meth. A* **91–96**, 621 (2010). <https://doi.org/10.1016/j.nima.2010.06.097>
23. Y.W. Yang, Z.W. Wen, Z.J. Han et al., A multi-cell fission chamber for fission cross-section measurements at the back-n white neutron beam of CSNS. *Nucl. Instrum. Meth. A* **486–491**, 940 (2019). <https://doi.org/10.1016/j.nima.2019.06.014>
24. J. Wen, Y.W. Yang, Z.W. Wen et al., A multi-layered fast ionization chamber prototype for fission cross section measurements. *J. Instrum.* **13**(07), P07020 (2018). <https://doi.org/10.1088/1748-0221/13/07/P07020>
25. X.Y. Liu, Y.W. Yang, R. Liu et al., Measurement of the neutron total cross section of carbon at the back-n white neutron beam of CSNS. *Nucl. Sci. Tech.* **30**, 139 (2019). <https://doi.org/10.1007/s41365-019-0660-9>
26. A.D. Carlson, V.G. Pronyaev, R. Capote et al., Evaluation of the neutron data standards. *Nucl. Data Sheets* **148**, 143–188 (2018). <https://doi.org/10.1016/j.nds.2018.02.002>
27. Y.H. Chen, G.Y. Luan, J. Bao et al., Neutron energy spectrum measurement of the Back-n white neutron source ES#2 at CSNS. *Eur. Phys. J. A* **55**, 7 (2019). <https://doi.org/10.1140/epja/i2019-12808-1>
28. Q. Wang, P. Cao, X. Qi et al., General-purpose readout electronics for white neutron source at China spallation neutron source. *Rev. Sci. Instrum.* **89**(1), 013511 (2018). <https://doi.org/10.1063/1.5006346>
29. J. Wen, Y. Yang, Z. Han et al., Accurate quantification of high purity uranium in coatings by small solid angle method. *Appl. Radiat. Isot.* **164**, 109300 (2020). <https://doi.org/10.1016/j.apradiso.2020.109300>
30. Z.Z. Ren, Y.W. Yang, J. Wen et al., Measurement of the $^{236}\text{U}(n, f)$ cross section for neutron energies from 0.4 MeV to 40 MeV from the back-streaming white neutron beam at the China spallation neutron source. *Phys. Rev. C* **102**, 034604 (2020). <https://doi.org/10.1103/PhysRevC.102.034604>
31. R. Brun, F. Rademakers, ROOT—an object oriented data analysis framework. *Nucl. Instrum. Meth. A* **389**, 81 (1997). [https://doi.org/10.1016/S0168-9002\(97\)00048-X](https://doi.org/10.1016/S0168-9002(97)00048-X)
32. J.A. Grundl, D.M. Gilliam, N.D. Dudev et al., Measurement of absolute fission rates. *Nucl. Technol.* **25**(2), 237–257 (1975). <https://doi.org/10.13182/NT75-A24366>
33. P.H. White, Alpha and fission counting of thin foils of fissile material. *Nucl. Instrum. Methods* **79**, 1–12 (1970). [https://doi.org/10.1016/0029-554X\(70\)90002-9](https://doi.org/10.1016/0029-554X(70)90002-9)
34. Z.Z. Ren, Y.W. Yang, R. Liu et al., Measurement of the $^{236,238}\text{U}(n, f)$ cross sections from the threshold to 200 MeV at CSNS Back-n. *Eur. Phys. J. A* **59**, 5 (2023). <https://doi.org/10.1140/epja/s10050-022-00910-8>
35. J.F. Briesmeister, *MCNP-A general Monte Carlo N particle transport code, LA-13709-M* (Los Alamos National Laboratory, Los Alamos, 2000)
36. J. Wen, Y.W. Yang, Z.W. Wen et al., Measurement of the U-238/U-235 fission cross section ratio at CSNS—back-n WNS. *Ann. Nucl. Energy* **140**, 107301 (2020). <https://doi.org/10.1016/j.anucene.2019.107301>
37. X.R. Hu, G.T. Fan, W. Jiang et al., Measurements of the $^{197}\text{Au}(n, \gamma)$ cross section up to 100 keV at the CSNS Back-n facility. *Nucl. Sci. Tech.* **32**, 101 (2021). <https://doi.org/10.1007/s41365-021-00931-w>
38. J.S. Zhang, UNF code for fast neutron reaction data calculations. *Nucl. Sci. Eng.* **142**, 2 (2002). <https://doi.org/10.13182/NSE02-02>
39. ADS-HE, IAEA. <https://www-nds.iaea.org/exfor/endl.htm>

Springer Nature or its licensor (e.g. a society or other partner) holds exclusive rights to this article under a publishing agreement with the author(s) or other rightsholder(s); author self-archiving of the accepted manuscript version of this article is solely governed by the terms of such publishing agreement and applicable law.

Authors and Affiliations

Zhi-Zhou Ren^{1,2}  · Yi-Wei Yang² · Yong-Hao Chen^{3,4}  · Rong Liu² · Bang-Jiao Ye¹ · Jie Wen² · Hai-Rui Guo⁵  · Zi-Jie Han² · Qi-Ping Chen² · Zhong-Wei Wen² · Wei-Li Sun⁵ · Han Yi^{3,4} · Xing-Yan Liu² · Tao Ye⁵  · Jiang-Bo Bai² · Qi An^{1,6} · Jie Bao⁷ · Yu Bao^{3,4} · Ping Cao^{6,8} · Hao-Lei Chen^{1,6} · Zhen Chen^{1,6} · Zeng-Qi Cui⁹ · Rui-Rui Fan^{3,4,10} · Chang-Qing Feng^{1,6}  · Ke-Qing Gao^{3,4} · Xiao-Long Gao^{3,4} · Min-Hao Gu^{3,10} · Chang-Cai Han¹¹ · Guo-Zhu He⁷ · Yong-Cheng He^{3,4}  · Yang Hong^{3,4,12} · Yi-Wei Hu⁹ · Han-Xiong Huang⁷ · Xi-Ru Huang^{1,6} · Hao-Yu Jiang⁹ · Wei Jiang^{3,4} · Zhi-Jie Jiang^{1,6} · Han-Tao Jing^{3,4} · Ling Kang^{3,4} · Bo Li^{3,4} · Chao Li^{1,6} · Jia-Wen Li^{6,13} · Qiang Li^{3,4} · Xiao Li^{3,4}  · Yang Li^{3,4} · Jie Liu⁹ · Shu-Bin Liu^{1,6} · Ze Long^{3,4} · Guang-Yuan Luan⁷ · Chang-Jun Ning^{3,4} · Meng-Chen Niu^{3,4} · Bin-Bin Qi^{1,6} · Jie Ren⁷  · Xi-Chao Ruan⁷ · Zhao-Hui Song¹¹ · Kang Sun^{3,4,12} · Zhi-Jia Sun^{3,4,10} · Zhi-Xin Tan^{3,4} · Jing-Yu Tang^{6,8}  · Xin-Yi Tang^{1,6} · Bin-Bin Tian^{3,4} · Li-Jiao Wang^{3,4,12}  · Peng-Cheng Wang^{3,4} · Zhao-Hui Wang⁷ · Xiao-Guang Wu⁷ · Xuan Wu^{3,4} · Li-Kun Xie^{6,13} · Xiao-Yun Yang^{3,4} · Li Yu^{3,4} · Tao Yu^{1,6} · Yong-Ji Yu^{3,4} · Guo-Hui Zhang⁹ 

Lin-Hao Zhang^{3,4,12} · Qi-Wei Zhang⁷ · Xian-Peng Zhang¹¹ · Yu-Liang Zhang^{3,4} · Zhi-Yong Zhang^{1,6} · Lu-Ping Zhou^{3,4,12} · Zhi-Hao Zhou^{3,4,12} · Ke-Jun Zhu^{3,10,12}

✉ Rong Liu
liurongzy@163.com

¹ Department of Modern Physics, University of Science and Technology of China, Hefei 230026, China

² Institute of Nuclear Physics and Chemistry, China Academy of Engineering Physics, Mianyang 621900, China

³ Institute of High Energy Physics, Chinese Academy of Sciences (CAS), Beijing 100049, China

⁴ Spallation Neutron Source Science Center, Dongguan 523803, China

⁵ Institute of Applied Physics and Computational Mathematics, Beijing 100088, China

⁶ State Key Laboratory of Particle Detection and Electronics, University of Science and Technology of China, Hefei 230027, China

⁷ Key Laboratory of Nuclear Data, China Institute of Atomic Energy, Beijing 102413, China

⁸ School of Nuclear Science and Technology, University of Science and Technology of China, Hefei 230027, China

⁹ State Key Laboratory of Nuclear Physics and Technology, School of Physics, Peking University, Beijing 100871, China

¹⁰ State Key Laboratory of Particle Detection and Electronics, Institute of High Energy Physics, Chinese Academy of Sciences, Beijing, China

¹¹ Northwest Institute of Nuclear Technology, Xi'an 710024, China

¹² University of Chinese Academy of Sciences, Beijing 100049, China

¹³ Department of Engineering and Applied Physics, University of Science and Technology of China, Hefei 230026, China